A Study of Convection Through Experimentation and Case Studies

Vince Agard

April 2009

Abstract

In this study, convection is examined in water through laboratory experimentation, and in the atmosphere through analysis of meteorological data. Potential and equivalent potential temperature are applied to case studies of dry and moist atmospheric convection, and it is concluded that the laboratory experiments conducted create situations analogous to these cases.

1 Introduction and theory

During the daytime, the Earth's troposphere is heated from the bottom by solar radiation striking the planet's surface, while it is cooled from the top by outgoing terrestrial re-radiation. This sometimes causes air parcels at the surface to become more buoyant than those in the upper troposphere, leading to overturning circulation in the form of dry or moist convection. The convective motions that establish equilibrium in the atmosphere are studied using laboratory experiments in which a tank of water is heated from the bottom, leading to vertical instability and overturning motions analogous to those in the atmosphere.

1.1 Convection in an incompressible fluid

Aside from scale, the primary difference between the convection in the laboratory experiments and convection in the atmosphere is the incompressibility of water. While water is an almost-incompressible fluid, the air in the atmosphere is quite compressible. For the purpose of studying convection, water is taken to be incompressible in the sense that its density is independent of pressure. However, it is important to consider that the density of water is dependent upon its temperature, since the buoyancy of a water parcel is dependent

on differences in density between the parcel and its surroundings. In the case of water, the relationship between temperature and density can be approximated as

$$\rho = \rho_{ref}(1 - \alpha T), \tag{1}$$

where ρ is the density of the fluid, ρ_{ref} is a constant reference density, and α is the coefficient of thermal expansion of water (Illari & Marshall, 2009).

Considering a horizontally uniform body of water with vertical density gradient $\frac{d\rho}{dz}$, one can determine the motions of fluid parcels undergoing adiabatic displacement. If a parcel with initial temperature T_0 and density ρ_0 is moved adiabatically upward within the fluid by distance δz, it will retain its temperature, and since density is dependent only on temperature, its density will also remain constant. However, the density of the surrounding fluid ρ_e will be different from ρ_0 as dictated by the environmental density gradient:

$$\rho_e = \rho_0 + (\frac{d\rho}{dz})\delta z. \tag{2}$$

This first order approximation holds well for small values of the displacement δz. Since the buoyancy of a water parcel is given by the difference between its density and the density of the surrounding fluid, it can be stated that the displaced parcel will be

$$\left.\begin{array}{c}\text{positively}\\ \text{neutrally}\\ \text{negatively}\end{array}\right\} \text{buoyant if } \frac{d\rho}{dz} \left\{\begin{array}{l} > 0 \\ = 0 \\ < 0 \end{array}\right. . \tag{3}$$

If the displaced parcel is positively buoyant, it will continue to accelerate upward through the fluid, while a negatively buoyant parcel will fall back down. A fluid in which parcels attain large displacements after slight perturbations is considered to be unstable. Therefore, the stability of the water column can be expressed as

$$\left.\begin{array}{c}\text{unstable}\\ \text{neutral}\\ \text{stable}\end{array}\right\} \text{if } \frac{d\rho}{dz} \left\{\begin{array}{l} > 0 \\ = 0 \\ < 0 \end{array}\right. . \tag{4}$$

Using Eq. (1), this can also be expressed as

$$\left.\begin{array}{c}\text{unstable}\\ \text{neutral}\\ \text{stable}\end{array}\right\} \text{if } \frac{dT}{dz} \left\{\begin{array}{l} < 0 \\ = 0 \\ > 0 \end{array}\right. , \tag{5}$$

where $\frac{dT}{dz}$ is the vertical temperature gradient of the water (Illari & Marshall, 2009).

1.2 Mixed layer

In a column of water that is made unstable by heating from the bottom, convection will take place through the column to the height at which the fluid is no longer unstable. Therefore, if there is a layer of water that is stable to convection, the convective motions will be unable to penetrate this layer. The bottom, convective layer of the fluid is referred to as the mixed layer, since the overturning circulations in this layer will cause the fluid to become well-mixed and of uniform temperature. Depending on the overall density distribution of the water column, the height reached by the mixed layer can change over time as convection evolves.

2 Tank experiments

2.1 Methods

To investigate convection in the lab, two tank experiments were performed. In each experiment, a heating pad was placed at the base of a large, plastic tank, as seen in Fig. 1. Five temperature sensors were placed at heights of 3 cm, 9 cm, 15 cm, 21 cm, and 27 cm each along one face of the tank. The tank was then filled with water. The ways in which the water was distributed vertically in the tank differed between the two experiments.

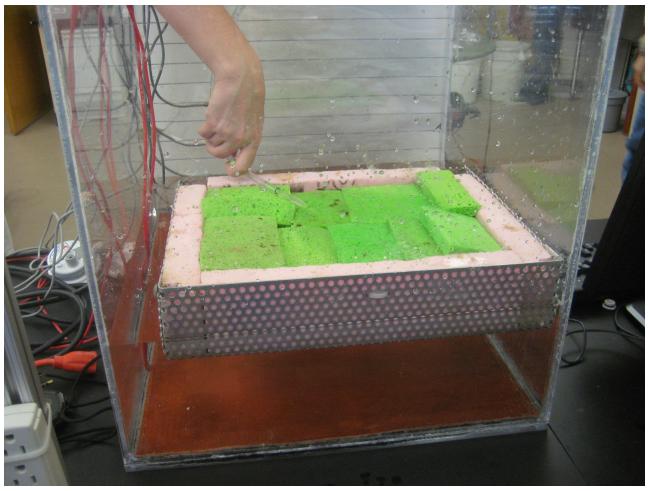

Figure 1: Setup of the lab experiments. Water is being poured slowly over the sponge apparatus, which helps prevent vertical mixing of the water column. The orange heating pad is at the bottom of the tank, and the temperature sensors can be seen taped to the far side of the tank.

Two-layer density difference experiment In this experiment, two layers of water with differing densities were deposited in the tank. The bottom layer was made to be more dense through mixing of salt, with an initial density of 1013 g/cm^3. The top layer was composed of less dense fresh water. These layers were using the sponge apparatus as seen in Fig. 1 to ensure minimal initial mixing between the layers.

Temperature-stratified experiment In this experiment, layers of water of different temperature were used to create an initial temperature profile that increased approximately linearly with height. Layers of water with temperatures of 23°C, 29°C, 32°C, 35°C, 38°C, and 45°C were also created in the tank using the sponge apparatus to ensure minimal initial mixing between the layers. However, since the layers were all in thermal contact, it was assumed that the temperature profile had become relatively continuous by the start of the experiment.

After the water was deposited in the tank, the heating pad was turned on, and potassium permanganate dye was added to the water. This dye allowed convective motions to be observed in the mixed layer. For ease of viewing, the tank was lit from behind and one side was covered with a piece of paper, as seen in Fig. 2. For each experiment, temperature data from each of the sensors, mixed layer height data, and estimated plume speed data were collected.

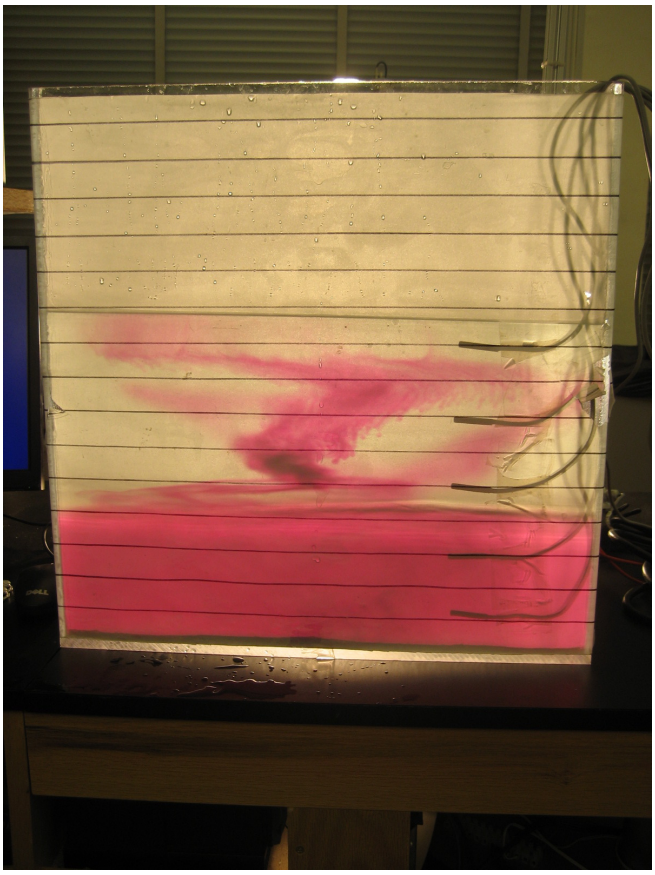

Figure 2: The temperature-stratified experiment in progress. The solid-colored bottom layer indicates the mixed layer, in which convection is taking place. The tank is covered with a piece of paper, and illuminated from behind. The shadows of the temperature sensors can be seen on the right side of the paper.

2.2 Results of the two-layer density difference experiment

For the two-layer experiment, a plot was generated showing the temperatures at each of the sensors versus elapsed time. This plot is shown in Fig. 3.

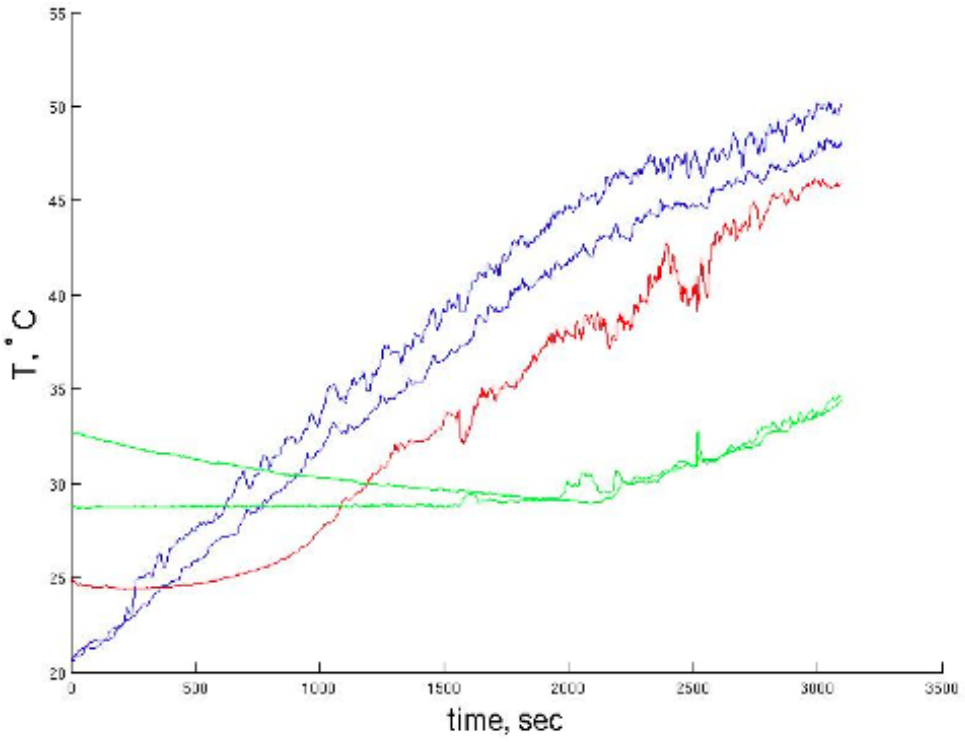

Figure 3: Temperature data are plotted versus elapsed time for the density-layered experiment. Color-coding denotes data from each of the different temperature sensors.

Additionally, an energy budget was conducted for the convective layer in this experiment using the equation

$$P = \frac{\partial H}{\partial t} = \rho_{ref} c_p \frac{\partial T}{\partial t} h l^2, \tag{6}$$

where P is the power used by the convective layer, H is the total heat in the mixed layer, h is the height of the mixed layer, and l is the length of one side of the base of the square tank. For this calculation, the temperature increase of water in the mixed layer was taken to be linear, at a constant rate of $\frac{\partial T}{\partial t} = 0.0107$K/s. The reference density ρ_{ref} was taken as 1 g/cm^3, and the specific heat capacity of water was used as $c_p = 4.19$J/g/K. The measured height of the mixed layer of 14 cm was used, as well as the measured length of an edge of the tank, 46cm. These data yield a value of 1330 W power in the mixed layer. The input power of the heating pad was 1620 W.

2.3 Discussion of density-layered experimental results

The temperature data for the density-layered experiment yielded many of the expected results. The mixed layer maintained a constant height for most of the experimental time window, and the temperature sensors well inside the mixed layer exhibited a linear pattern of temperature increase. This linear pattern can be seen in Fig. 3 in the two tracks whose temperatures start around 20°C. These tracks represent the bottom two temperature sensors, which were placed well inside the mixed layer. The red track represents a sensor which was positioned at the interface between the convecting mixed layer and the stable top layer. This track initially shows a constant progression, but then begins to increase linearly around 1000 s, when the top of the mixed layer has overtaken the height of the sensor. However, the temperature recorded by this sensor is consistently lower than that of the lower two sensors. This is likely due simply to the fact that this sensor is further from the heating pad, and there is additional heat loss due to transfer to the stable layer.

The top two sensors were placed in the stable top layer. These sensors initially start at two different temperatures, but are convergent until about 2000 seconds. However, after this time, the temperatures begin to increase linearly, suggesting that there is heat transfer from the convecting mixed layer. This is consistent with the fact that the mixed layer temperatures began to increase at a more shallow slope at the same time. However, during the experiment, there were no plumes visible breaking through the top of the mixed layer. Therefore, the way in which heat transfer between layers suddenly began remains uncertain.

Finally, the heat budget conducted for this experiment yields reasonable results. The calculated figure of 1330 W used in the mixed layer is relatively close to the actual power input of 1620 W. In fact, the fact that the calculated power value is slightly less than the input power is consistent with the fact that some of the power was lost to the upper layers.

2.4 Results of the temperature-stratified experiment

For the two-layer experiment, a plot was generated showing the temperatures at each of the sensors versus elapsed time. This plot is shown in Fig. 4. Shown in Fig. 5 is a plot showing the observed height of the convective mixed layer over time.

Additionally, plots were generated showing the natural log of temperature and the natural log of mixed layer height versus the natural log of time, shown in Figs. 6 and 7. These plots were generated to determine the way in which height and temperature evolve with time. The expected evolution of these values with time can be derived from the horizontally averaged thermodynamic equation

$$\rho c_p \frac{dT}{dt} = \frac{\mathcal{H}}{h}, \tag{7}$$

where c_p is the specific heat capacity of the fluid, $\mathcal{H}$ is the heat flux entering the tank from the heating pad, and h is the height of the convective mixed layer. With the assumption that temperature is constant within the mixed layer and consistent with the linear temperature profile at the top of the layer, temperature can be written as $T = \bar{T}_z h$. Substitution into Eq. (7) yields

$$\frac{1}{2}\rho c_p \bar{T}_z \frac{d}{dt} h^2 = \mathcal{H}. \tag{8}$$

This equation can be solved for h to yield

$$h = \sqrt{\frac{2\mathcal{H}t}{\rho c_p \bar{T}_z}}, \tag{9}$$

and since T is proportional to h, it can be concluded that both T and h evolve as $t^{\frac{1}{2}}$ (Illari & Marshall, 2009).

Therefore, in both the $\ln T$ vs. $\ln t$ and $\ln h$ vs. $\ln t$ plots, the data are expected to have linear form, with slope of $\frac{1}{2}$.

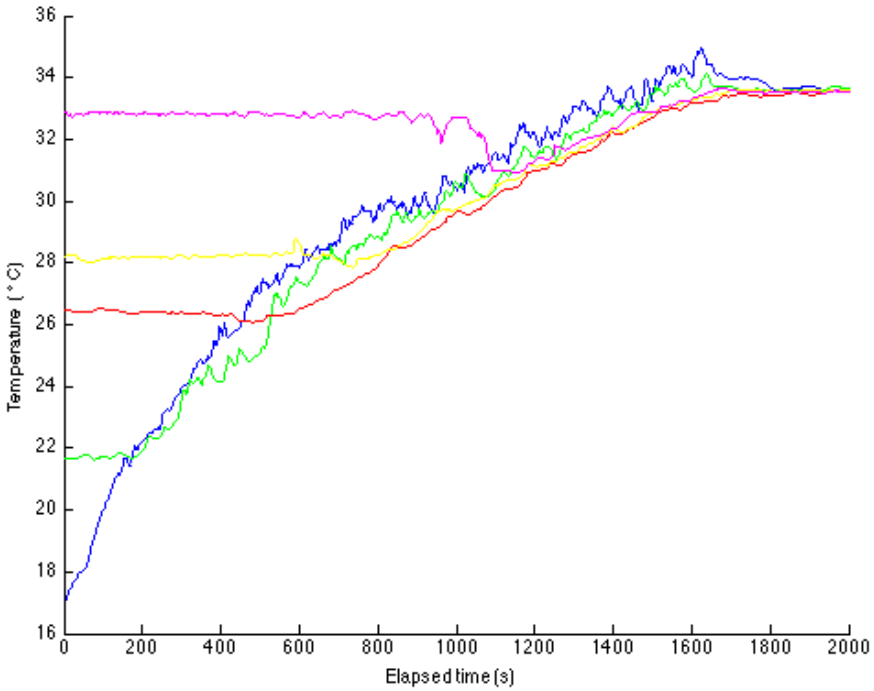

Figure 4: Temperature data are plotted versus elapsed time for the temperature-stratified experiment. The colored curves represent data from each of the sensors.

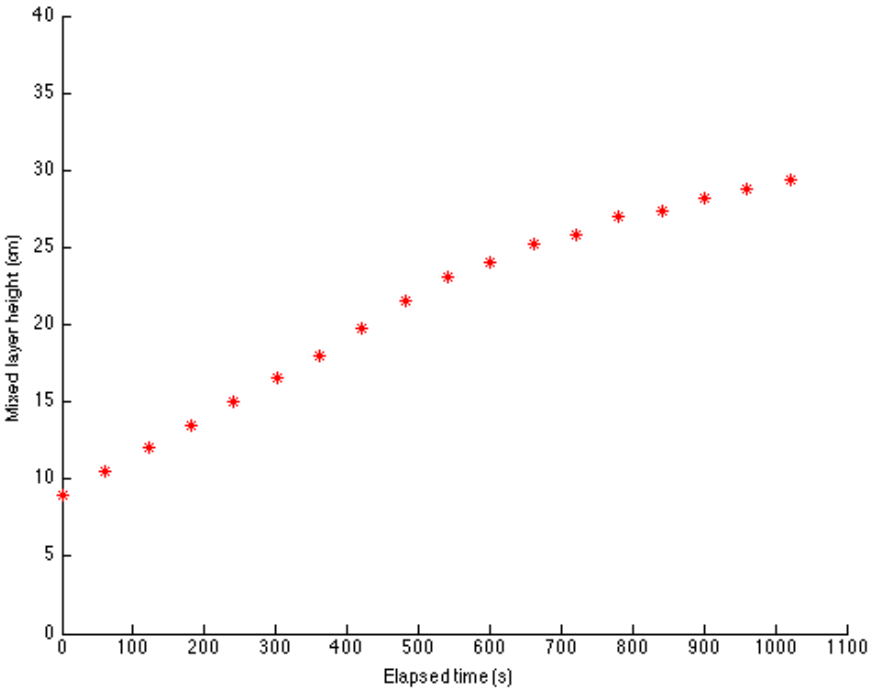

Figure 5: Mixed layer height data is plotted versus elapsed time for the temperature-stratified experiment.

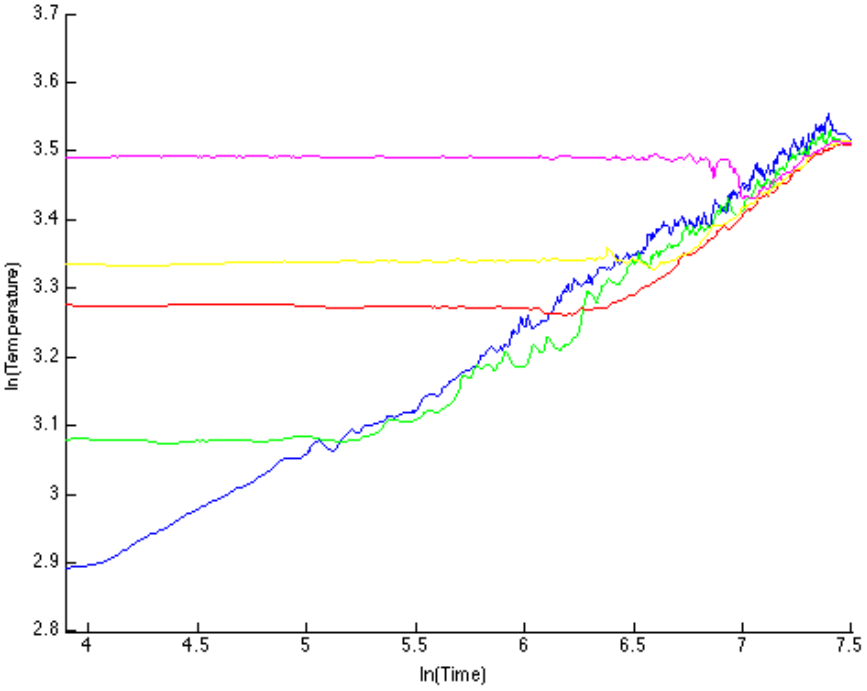

Figure 6: The natural logs of temperature data are plotted versus the natural log of elapsed time for the temperature-stratified experiment. The colored curves represent data from each of the sensors.

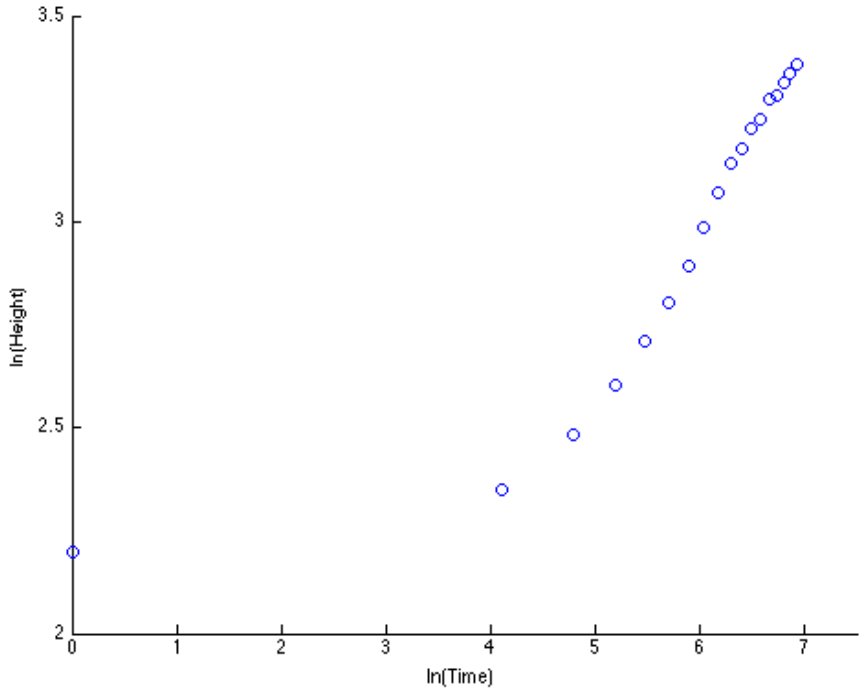

Figure 7: The natural log of mixed layer height data is plotted versus the natural log of elapsed time for the temperature-stratified experiment.

2.5 Discussion of temperature-stratified experimental results

The temperature data for the temperature-stratified experiment also yielded many of the expected results. The evolution of the mixed layer is visible in Fig. 4, as each temperature sensor enters the mixed layer in sequence. For each temperature sensor, the temperature remains relatively constant over time before the mixed layer height eclipses the height of the sensor. At this point, the temperature of each sensor begins to increase at the same rate as that of the other sensors. Likewise, for each temperature sensor inside the mixed layer, the instantaneous temperature values are nearly the same. This is caused by the convective motions of the mixed layers, which make uniform the temperature distribution throughout the layer.

Another expected result is shown in Fig. 6, as the data in the logarithmic plot of temperature versus time exhibits a linear relationship. The linearity of the data in this plot provides evidence that temperature evolves as a power function of time. However, the slope of the data in this plot is considerably less than $\frac{1}{2}$; instead the estimated slope is around $\frac{1}{4}$. This error could be caused by an initial temperature profile which was non-linear in the vertical.

The mixed layer height data in Fig. 5 show clearly the evolution of the convective mixed layer over time, as the boundary between stable and convective layers gains height as time elapses. However, the logarithmic plot of height versus time in Fig. 7 shows a non-linear relationship between $\ln h$ and $\ln t$. Again, this unexpected result could have been caused by non-linearity in the initial temperature profile. Indeed, the initial temperature profile was non-linear, as the initial temperatures of the layers were 23, 29, 32, 35, 38, and 45 °C, respectively. This inconsistency in temperature differences between layers may have been responsible for the non-linear nature of the data seen here. This notion is further supported by the apparent "kink" in the height data in Fig. 5 at approximately 550 seconds, at which the rate at which the mixed layer height rises appears to change abruptly.

In each of the experiments, the temperature plots of those sensors inside the mixed layer exhibit a noisy, up-and-down pattern. This pattern is consistent with the upward movement of warm, buoyant water parcels past the temperature sensors in contrast with the downward movement of cool, negatively buoyant parcels. This explanation is supported by the fact that the temperature variations are larger toward the bottom of the tank, where sensors are closer to the heating pad, and therefore plumes are larger.

3 Atmospheric data analysis

Convection in the atmosphere exhibits many of the same properties exhibited by the laboratory experiments conducted. While the tank experiments featured a water column being

warmed from below by a heating pad, atmospheric convection features a column of air being warmed from below by solar radiation. Likewise, in either case, convection occurs to a certain mixed layer height, resulting a uniform temperature distribution in the mixed layer. These similarities are illustrated in Fig. 8.

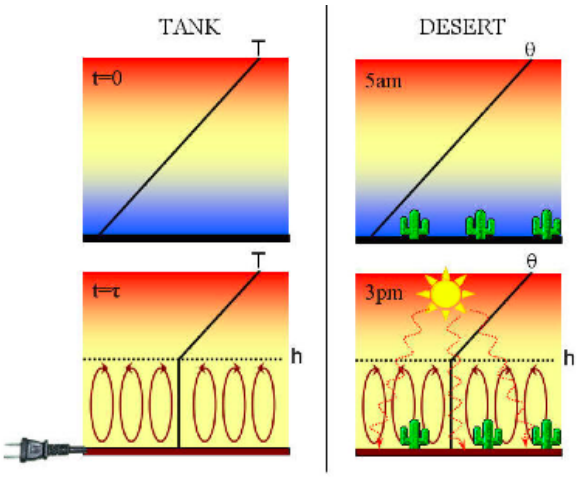

Figure 8: Comparison of the temperature-stratified lab experiment with dry atmospheric convection in the desert (Tang, 2009).

3.1 Dry convection

The key difference between atmospheric convection and convection in water is that the atmosphere is a compressible fluid. The compressibility of the air causes air parcels displaced upward to cool as they move adiabatically. The rate at which the air parcels cool adiabatically with height in a dry atmosphere is the dry adiabatic lapse rate:

$$\Gamma_d = -\frac{g}{c_p} = 10^{\circ}\mathrm{K/km}. \tag{10}$$

This lapse rate defines a new stability criteria for the dry atmosphere:

$$\left.\begin{array}{c}\text{unstable}\\ \text{neutral}\\ \text{stable}\end{array}\right\} \text{if } \frac{dT}{dz} \left\{\begin{array}{l} < -\Gamma_d \\ = -\Gamma_d \\ > -\Gamma_d \end{array}\right. . \tag{11}$$

To further clarify the analogy to convection in compressible fluids, it is useful to define a quantity called potential temperature as

$$\theta = T\left(\frac{p_0}{p}\right)^{\kappa}, \tag{12}$$

where p_0 is a constant reference pressure and $\kappa = \frac{R}{c_p} = \frac{2}{7}$. Now, the stability criteria for a dry atmosphere can be written as

$$\left.\begin{array}{c}\text{unstable}\\ \text{neutral}\\ \text{stable}\end{array}\right\} \text{if } \frac{d\theta}{dz} \begin{cases} < 0 \\ = 0 \\ > 0 \end{cases} . \tag{13}$$

Thus, θ for a dry atmosphere is analogous to T for an incompressible fluid, as both are adiabatically conserved quantities whose vertical gradients determine stability of the fluid.

3.1.1 Dry atmospheric convection case study

To study dry convection in the atmosphere, a case study was undertaken of a hot summer day in Yuma, Arizona. With little moisture in the air on June 18, 2007, solar heating of the surface to temperatures of up to 107°F lead to dry convection as the day progressed. Instantaneous temperature data for different points through the troposphere were available for six times from 4:36 AM to 2:39 PM local time. Using these data, profiles of temperature and potential temperature were plotted for each time. Temperature profiles are shown in Fig. 9, while potential temperature profiles are shown in Fig. 10.

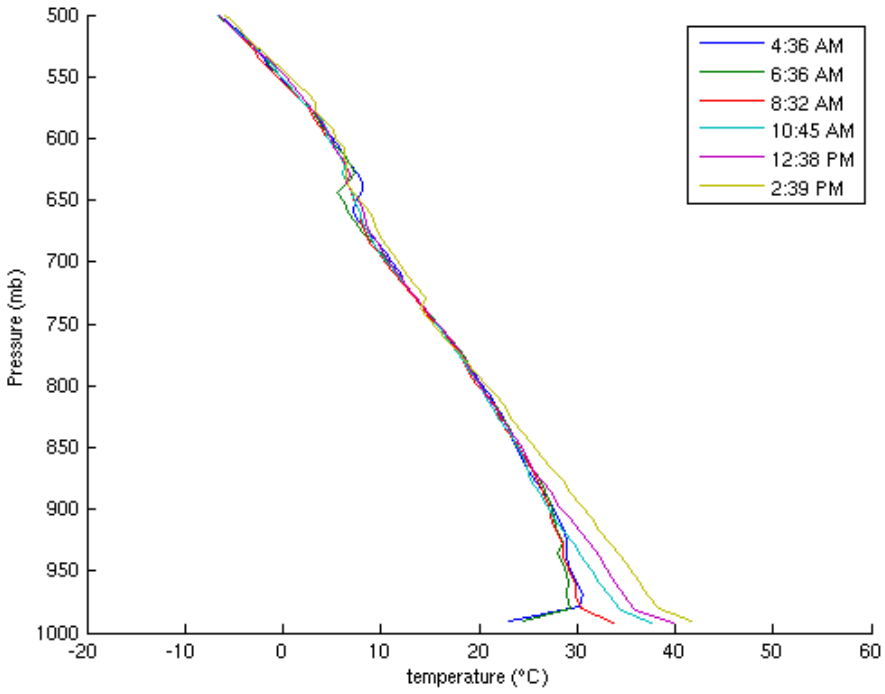

Figure 9: Temperature data are plotted versus height for six different times over the course of a day in Yuma, Arizona.

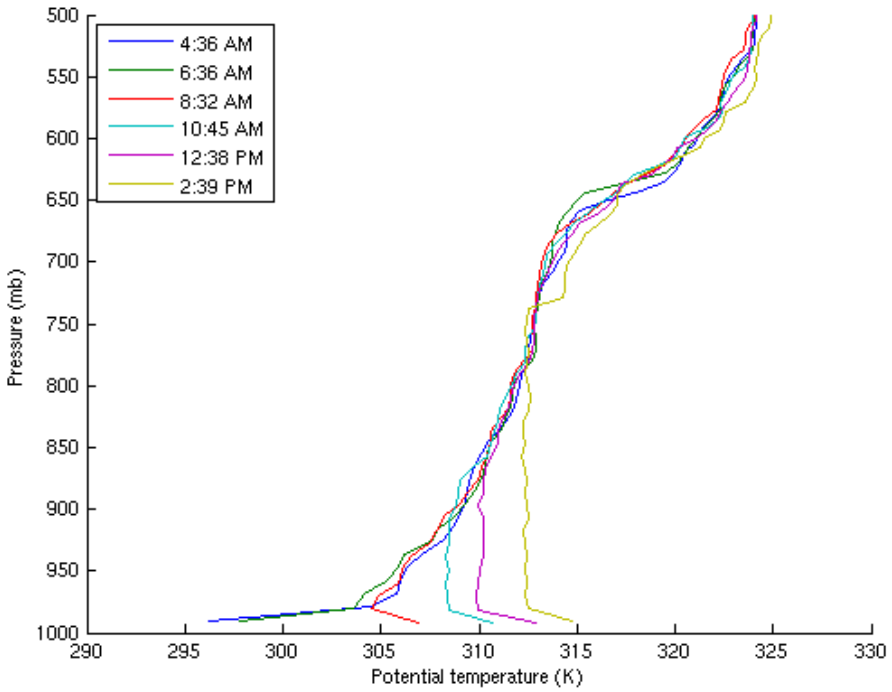

Figure 10: Potential temperature data are plotted versus height for six different times over the course of a day in Yuma, Arizona.

Additionally, a similar heat budget to the one conducted for the lab experiment can be conducted for this situation. Incoming solar radiation data can be compared to the calculated change in internal atmospheric energy using the equation

$$H = \int \rho c_p \frac{\partial T}{\partial t} dz = \frac{c_p}{g} \int_{p_s fc}^{p_b oundary} \frac{\partial T}{\partial t} dp. \tag{14}$$

To use this equation with the given data, the equation is used in its discrete form:

$$H\Delta t = \frac{\partial c_p}{\partial g} \sum_{i=1}^{N} \Delta T_i \delta p_i. \tag{15}$$

This equation was used to create a plot comparing observed solar radiation to calculated rate of heat inflow to the troposphere, which is shown in Fig. 11.

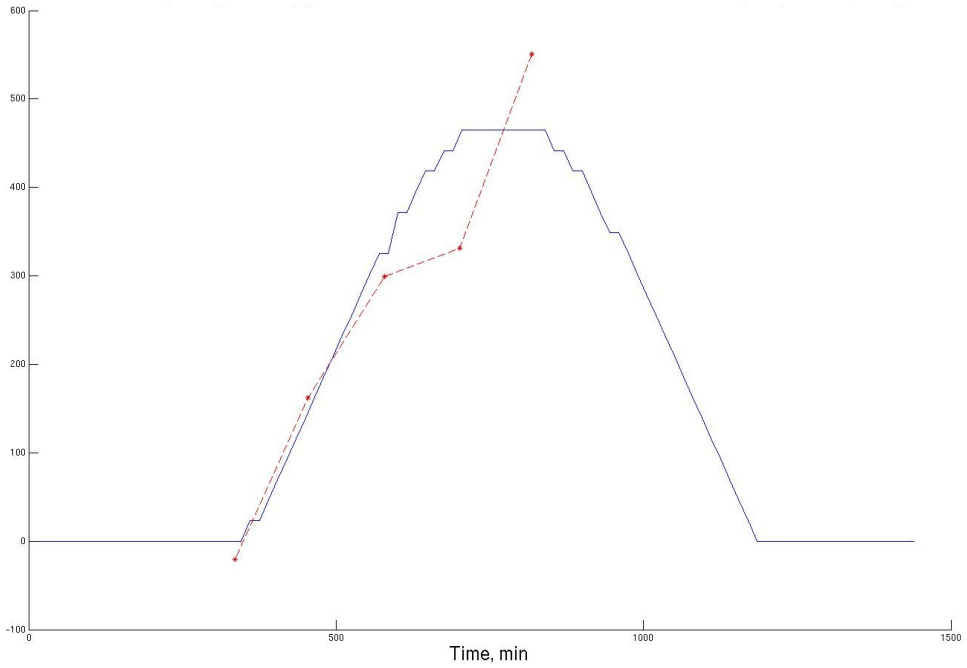

Figure 11: Observed incoming solar radiation (blue) and calculated rate of heat inflow to the troposphere (red) are plotted versus time over the course of a day in Yuma, Arizona.

3.1.2 Discussion of dry atmospheric convection data

The temperature profiles for Yuma, Arizona show temperature decreasing with height throughout the troposphere, as predicted by the compressibility of air. However, the plot in Fig. 9 is not very informative about the stability of the atmosphere. One noticeable feature of this plot is the nighttime surface cooling visible in the 4:36 AM and 6:36 AM temperature profiles. The increase in temperature with height close to the surface in these two profiles is consistent with overnight cooling of the surface, while the sharp decrease in temperature with height in later profiles shows surface warming due to solar radiation.

The potential temperature profiles are more informative about dry atmospheric convection taking place throughout the day. The nighttime cooling and daytime warming are still visible, but in addition, the profiles of potential temperature show the evolution of convective motions throughout the day. The last three profiles of the day show regions of vertically uniform potential temperature. In these regions, convection is taking place, mixing the bottom layer of the atmosphere, and causing the potential temperature to become uniform throughout this mixed layer. Additionally, in these three profiles, the evolution of the mixed layer height over time can be seen, as the region of uniform potential temperature extend further in the vertical as time progresses and the surface continues to be heated.

The plot of incoming solar radiation and calculated rate of heat inflow in Fig. 11 shows the rate of heat inflow to the troposphere to be quite comparable to the incoming solar radiation. The two curves follow the same general shape, and the magnitudes of each term were relatively close. Unfortunately, the lack of temperature data in the very early morning or late afternoon prevents further comparison of the two curves. However, given the available data, the two sides of the heat budget equation appear to follow each other very well.

3.2 Moist convection

While dry atmospheric convection can occur in hot, dry places such as the desert, in most locations the air contains a significant amount of water vapor. As a result, much of the atmospheric convection that takes place around the world is moist convection. In moist convection, air parcels being moved adiabatically upward through the atmosphere undergo a latent heat release as condensation occurs. As a result, the adiabatic lapse rate of a moist atmosphere is less than that of a dry atmosphere. In the case of a saturated atmosphere, adiabatically displaced parcels cool with height at the saturated adiabatic lapse rate

$$\Gamma_s = -\Gamma_s \left[\frac{1 + \frac{Lq_*}{RT}}{1 + \frac{\beta L q_*}{c_p}} \right], \tag{16}$$

where L is the latent heat of condensation and q_* is the saturation specific humidity.

It is now useful to define a new quantity called equivalent potential temperature as

$$\theta_e = \theta e^{\left(\frac{Lq}{c_p T}\right)}. \tag{17}$$

The stability criteria for a moist atmosphere can therefore be written as

$$\left.\begin{array}{c}\text{unstable}\\ \text{neutral}\\ \text{stable}\end{array}\right\} \text{if } \frac{d\theta_e}{dz} \begin{cases} < 0 \\ = 0 \\ > 0 \end{cases} . \tag{18}$$

Thus, θ_e for a moist atmosphere is analogous to *theta* for a dry atmosphere, and to T for an incompressible fluid, as all are adiabatically conserved quantities whose vertical gradients determine stability of the fluid (Marshall & Plumb, 2008).

3.2.1 Moist atmospheric convection case study

To study moist convection in the atmosphere, a case study was undertaken of a recent day in Charleston, South Carolina. On this day, surface heating through solar radiation took place through most of the day, with moist convection in the form of thunderstorms passing through in the evening hours. Instantaneous temperature and humidity data were used to create potential and saturated equivalent potential temperature profiles for four times from 8:00 AM to 11:00 PM over the course of a day. Potential temperature profiles are shown in Fig. 12. In this case, humidity data were unavailable, so a saturated atmosphere was assumed for simplicity. Therefore, profiles of saturated equivalent potential temperature ($\theta_{es} = \theta e^{\left(\frac{Lq_*}{c_p T}\right)}$) are shown in Fig. 13.

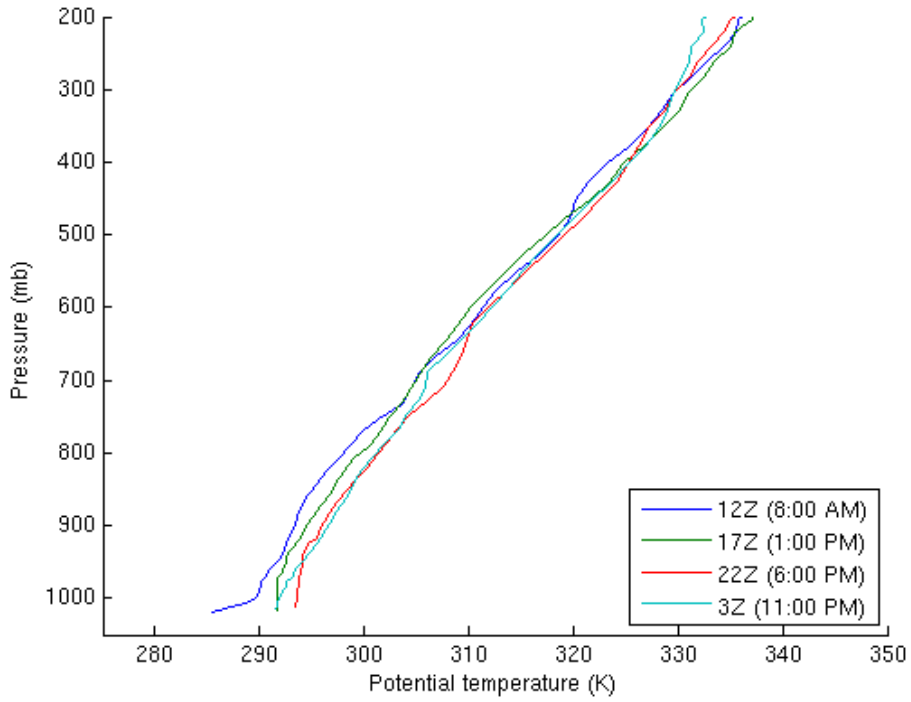

Figure 12: Potential temperature data are plotted versus height for four different times over the course of a day in Charleston, South Carolina.

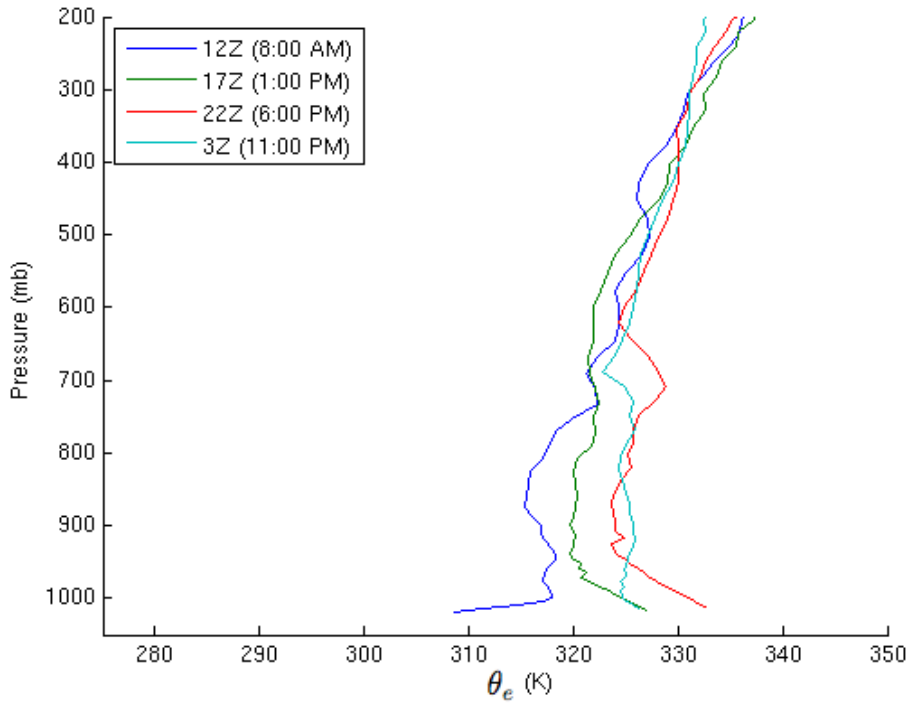

Figure 13: Saturated equivalent potential temperature data are plotted versus height for four different times over the course of a day in Charleston, South Carolina.

3.2.2 Discussion of moist atmospheric convection data

The potential temperature profiles shown in Fig. 12 are again not very informative. Potential temperature is seen to be increasing with height throughout the troposphere at each time. Therefore, if this were a dry atmosphere, it would be stable to convective motions. However, the presence of water vapor in the atmosphere enables moist convection to take place, as is demonstrated by the saturated equivalent potential temperature profiles in Fig. 13.

The profiles of saturated equivalent potential temperature are more informative about the stability of the atmosphere over the course of the day. At 8:00 AM, there is still strong evidence of nighttime surface cooling, as saturated equivalent potential temperature increases sharply with height at the surface. However, as the day progresses, solar radiation heats the surface, causing an unstable (decreasing with height) condition near the surface for the 1:00 PM and 6:00 PM profiles. However, the 11:00 PM profile shows saturated equivalent potential temperature values that are roughly uniform from the surface to the 750 mb level. This suggests that this layer has been mixed by moist convection between 6:00 PM and 11:00 PM. Indeed, this is confirmed by radar imagery, as seen in Fig. 14, showing convective thunderstorms beginning to pass over the Charleston area just before 6:00 PM.

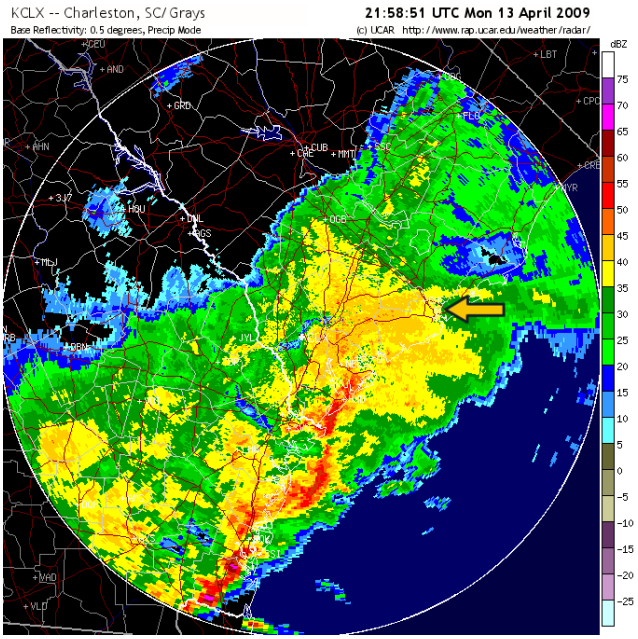

Figure 14: Base radar reflectivity image of convective precipitation in the area of Charleston, South Carolina at 5:58 PM on April 15, 2009. The arrow indicates the location of the weather station. (NCAR)

4 Conclusions

From this study, it can be concluded that convection can be observed both in compressible fluids such as the atmosphere, and in incompressible fluids such as water. Furthermore, atmospheric convection can occur in either a dry or moist air setting. In each of these situations, there is a quantity that is conserved in adiabatic motion whose vertical gradients determine the stability of the fluid. In the case of water, this quantity is temperature. In the case of a dry atmosphere, this quantity is potential temperature, and in the case of a moist atmosphere, this quantity is equivalent potential temperature. These quantities are analogous to each other, and each can predict the stability of its respective fluid to overturning convective motions.

It can also be concluded that the tank experiments conducted in this study are analogous to convection occurring in the atmosphere. In particular, the temperature-stratified experiment is especially analogous to dry atmospheric convection, as both feature an initially linear vertical temperature gradient which is mixed away through convective motions due to heating from the bottom. As time progresses, the height of the mixed layer in which there is a uniform temperature (or potential temperature) in each case becomes larger.

The heat budget conducted in the density-layered experiment was also analogous to the heat budget conducted for atmospheric convection. In each case, the heat inflow into the mixed layer was calculated to be comparable to the heat input to the system.

In future studies, the differences in magnitudes of temperature fluctuations between different levels in the tank experiment could be examined. The transfer of heat through the top of the mixed layer in the tank experiment prior to plume penetration of the boundary could also be studied. Additionally, convection in water could be further examined through different combinations of density and temperature strata.

5 References

Illari, Lodovica; Marshall, John. March 2009 - "12.307 Project 3: Convection"

Marshall, John; Plumb, R. Allen. 2008 - *Atmosphere, Ocean, and Climate Dynamics: An Introductory Text.* Elsevier.

Tang, Brian - "Yuma Convection Data Set" - 12.307 Weather and Climate Laboratory. http://paoc.mit.edu/12307/convection/yuma_instructions.htm - Last accessed April 22, 2009

"Radar Page: RAP Real-Time Weather" - The National Center for Atmospheric Research. http://rap.ucar.edu/weather/radar/ - Last accessed April 22, 2009